Bulletin of the Seismological Society of America, Vol. 86, No. 6, pp. 1681–1691, December 1996

A Monte Carlo Approach in Estimating Uncertainty for a Seismic Hazard Assessment of Los Angeles, Ventura, and Orange Counties, California

by Chris H. Cramer, Mark D. Petersen, and Michael S. Reichle

Abstract Maps of uncertainty and parametric sensitivity in ground motion have been produced for three southern California counties using a Monte Carlo approach. The uncertainty in hazard is estimated by random sampling a logic tree that has the uncertainty in most parameters described by a normal distribution. The nine parameters varied in the uncertainty analysis are those related to the estimation of recurrence rates for earthquakes on faults using geologic information, the ground-motion attenuation relations, the relations available for estimating the magnitude-frequency distribution of earthquakes on faults, and the inclusion or exclusion of blind thrusts in the Los Angeles area. Besides simultaneously varying all nine parameters for a Monte Carlo series of runs to obtain the overall uncertainty in ground motion for a fixed annual probability, each of the nine parameters were varied separately while the others were held fixed to determine the sensitivity of each parameter on this uncertainty. The total uncertainty in shaking levels corresponding to a fixed annual probability is up to $\pm 50\%$ at the 95% confidence level. The parameters that most influence the uncertainty in the hazard estimates from geologic information are (1) maximum magnitude, (2) choice of attenuation relations, (3) the magnitude-frequency distribution, and (4) slip rate.

Introduction

Following the 17 January 1994 Northridge earthquake (M_w 6.7), the California Governor's Office of Emergency Services (OES) and the Federal Emergency Management Administration (FEMA) asked the California Department of Conservation's Division of Mines and Geology (DMG) to assess the ground shaking hazard of Los Angeles, Ventura, and Orange counties (Petersen *et al.,* 1996). As a part of this assessment, an uncertainty analysis of the hazard analysis was undertaken. A Monte Carlo approach was coupled to a logic tree to perform the uncertainty analysis. The description of this approach and the results of the analysis are reported in this article.

The logic tree approach to uncertainty analysis is described by Coppersmith and Youngs (1986) and outlined in NRC (1988). McGuire and Shedlock (1981) previously produced an earthquake hazard uncertainty map for the San Francisco Bay area using a five-parameter discrete logic tree. Logic tree analyses generally have discrete probability distributions associated with each node in the tree, and uncertainty in the hazard for a fixed annual probability is assessed by using the conditional probability at the end of a branch and its associated probabilistic seismic hazard. In this article, most of the nodes have continuous probability distributions. So a Monte Carlo approach of randomly sampling the logic tree is used to simulate a distribution of hazard estimates from which specific percentile values are determined.

The original hazard maps produced by DMG for OES/FEMA (Petersen *et al.,* 1996) use the Poissonian source model developed by the Southern California Earthquake Center (SCEC) (Jackson *et al.,* 1995) supplemented with additional geological slip rates. The tri-county area (Ventura, Los Angeles, and Orange) and the relevant source faults and SCEC zones for the tri-county area are shown in Figure 1. Figure 2 shows the alluvial-site peak ground acceleration (PGA) hazard map for 10% exceedence in 50 yr from Petersen *et al.*'s probabilistic seismic hazard analysis (PSHA).

Method

To estimate uncertainty in the earthquake hazard related to the uncertainty in the geologic information used to develop the DMG hazard maps, a logic tree of relevant uncertainty parameters has been developed for the DMG hazard model for the tri-county area (Fig. 3). Petersen *et al.* incorporated style of faulting (normal, reverse, or strike-slip), fault dip, and fault or zone type (A, active fault with rupture history and a characteristic earthquake distribution; B, active fault with unknown rupture history and a 50% characteristic/50% Gutenberg–Richter earthquake distribution [differs from SCEC model]; and C, area of seismicity with no known active faults and a Gutenberg–Richter earthquake distribu-

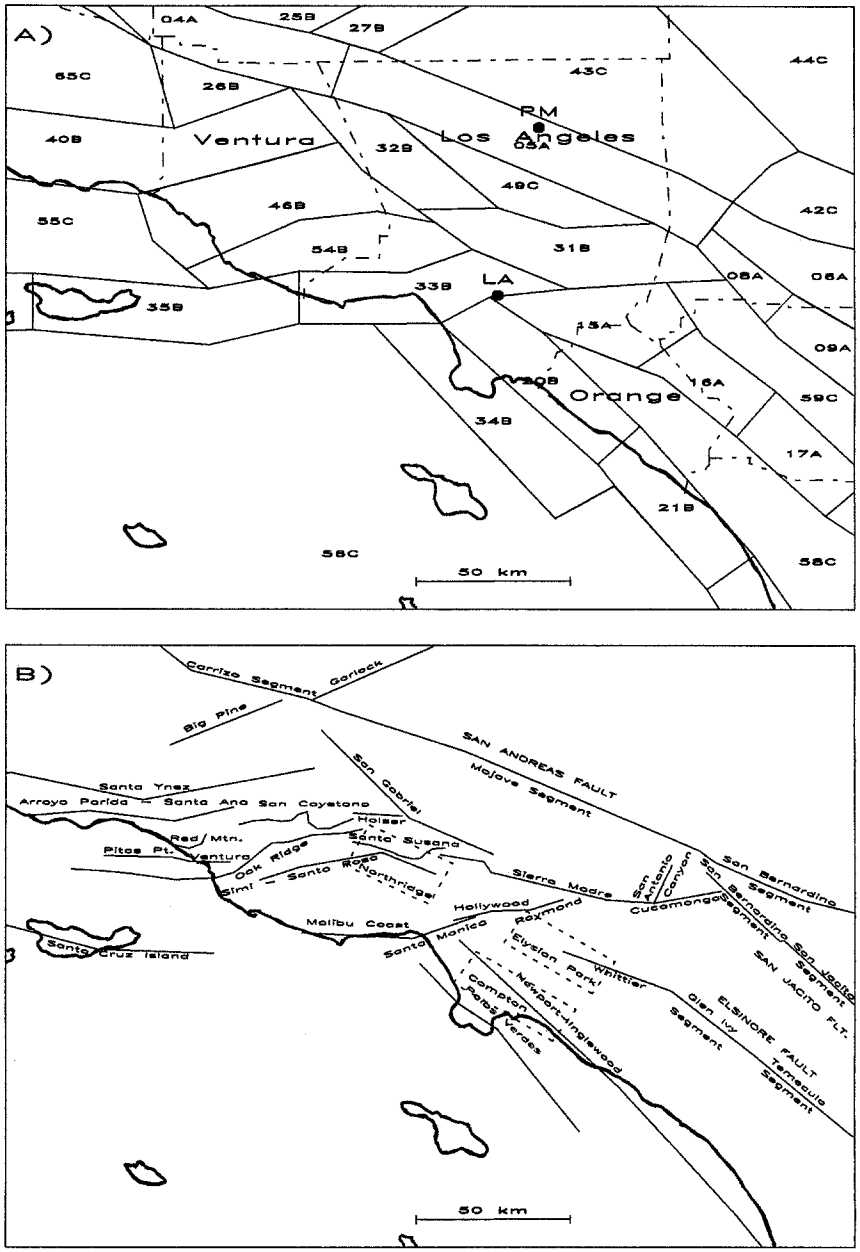

Figure 1. Maps of the tri-county study area showing (a) the geometry and classification of the zones modified from the SCEC model and the locations of Los Angeles (LA) and Palmdale (PM) referred to in Figure 4 and (b) the names and locations of faults used in the DMG model.

tion). This classification is fixed for each fault in the DMG model and is not included in the logic tree (Fig. 3).

Estimates of uncertainty in fault length, width, and slip rate are taken from Petersen *et al.* (1996) and Jackson *et al.* (1995). Estimates of uncertainty in *b*-value and the fault rupture length versus magnitude relation are taken from Reasenberg and Jones (1989) and Wells and Coppersmith (1994), respectively. The estimate of uncertainty in shear modulus is from the range of values of shear modulus in crustal rocks (3.0 to 3.5 $\times$ 10^{11} dyne/cm^2). Uncertainty in the value of shear modulus can contribute to uncertainty in hazard via the slip rate to activity-rate conversion, which involves the determination of the moment rate of a fault from geologic information (moment rate = shear modulus $\times$ fault length $\times$ fault width $\times$ slip rate) (see the section on How Uncertainty Depends on Hazard Value below).

Figure 3 shows nine parameters contributing to the overall uncertainty estimate. Most of these parameters represent epistemic uncertainties that contribute to the uncertainty in activity rates used in the hazard analysis as determined from geologic information. Six parameters have continuous uncertainty distributions, and three have discrete

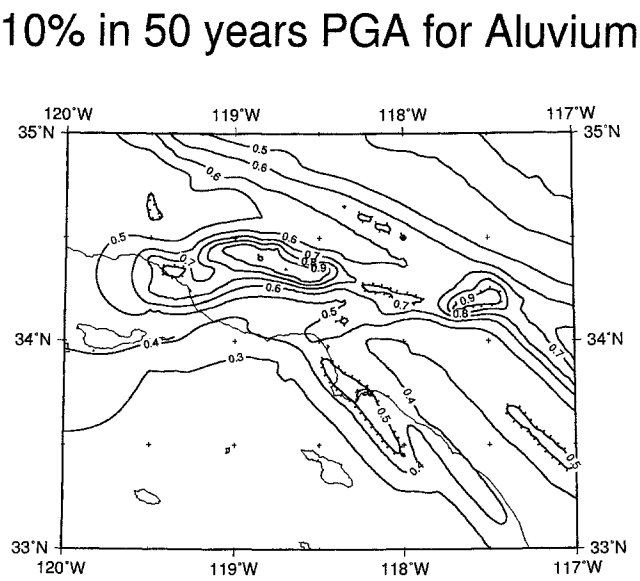

Figure 2. PSHA map of the tri-county area showing the peak ground acceleration (random horizontal component) exceeded at 10% in 50 yr exposure for alluvial site conditions. Ground-motion values are in units of the percentage of gravity (g) and the contour interval is 10% g. Local highs and lows are indicated by barbs to the outside (high) or inside (low) of the contour line.

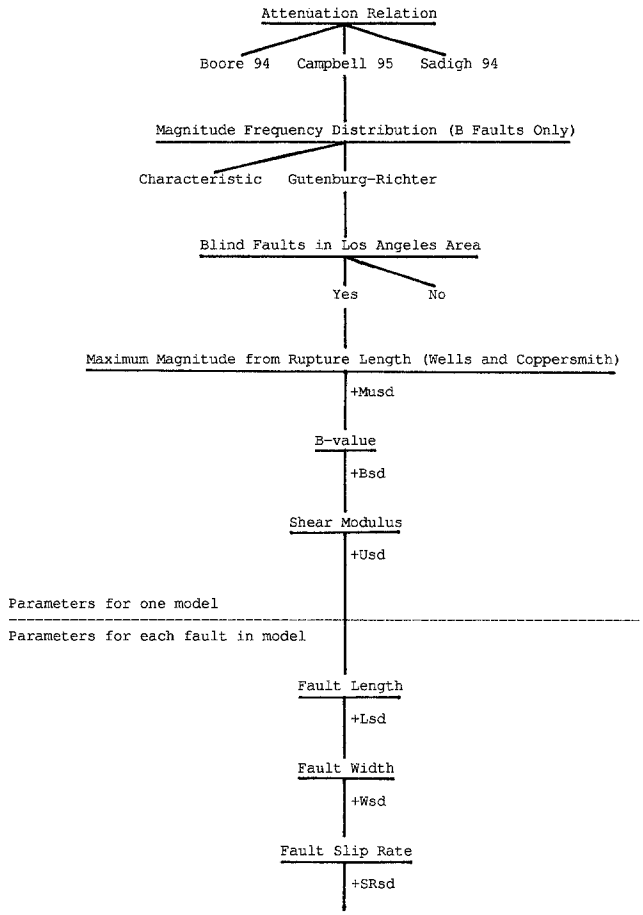

Figure 3. Uncertainty logic tree for the tri-county hazard analysis.

uncertainty distributions. All continuous uncertainty distributions are assumed to be normally distributed, and represented by a standard deviation (SD) about a mean value. The discrete uncertainty distributions assume equal weighting among the possible discrete outcomes.

Values and their uncertainties for the continuous distributions are as follows. Table 1 presents the value and SD for each fault's length and slip rate. Petersen *et al.* (1996) present ranges in values for estimates of uncertainty, and we assume that the ranges correspond to the 95% confidence limits (± 2 SD values) so that half the $\pm$ range value equals the SD shown in Table 1. The value of fault width of 11 km in Table 1 corresponds to the Ward (1994) geodetic moment-rate constraint on the seismogenic width adopted by Petersen *et al.*, while the ± 2-km SD in width is an estimate of its uncertainty. The mean and SD used for the shear modulus in this article is $3.3 \pm 0.1 \times 10^{11}$ dyne/cm^2. Petersen *et al.* use a b-value of 0.9, and Reasenberg and Jones provide an estimate for the SD in b-value of ± 0.2. Values for the SD in the subsurface fault rupture versus magnitude relations used to estimate the maximum magnitude earthquake that can occur on a fault were taken directly from Wells and Coppersmith (1994). (Note: Here Wells and Coppersmith provide an uncertainty estimate for the epistemic uncertainty in maximum magnitude that affects the activity rate of a fault.)

The discrete parameter distributions are as follows. For the B faults, the magnitude-frequency distribution can be either the characteristic or the Gutenberg–Richter model. For the attenuation relations, the three choices are Boore *et al.* (1993, 1994, 1994, written communication), Campbell and Bozorngia (1994), and Sadigh (1994, written communication). For the blind thrusts in the Los Angeles basin, the choice is to include or exclude them.

Moment magnitudes (M_w) have been used by Petersen *et al.* (1996). The relationship between moment magnitude and seismic moment is defined by Hanks and Kanamori (1979) and has no uncertainty. If magnitudes other than M_w are used in input parameters, then an additional uncertainty from a non-M_w magnitude versus seismic moment relationship must be added to the logic tree of Figure 3 and the Monte Carlo simulations.

We consider the uncertainty in the hazard from A and B faults only (Fig. 1), because their contribution dominates the hazard calculation near these faults. This is demonstrated in Figure 4, which shows separate hazard curves at two sites (Los Angeles and Palmdale) for the A faults, the B faults, background seismicity within the tri-county area, seismic sources outside the tri-county area, and the overall hazard curve for each site. For sites closer to B faults (e.g., Los Angeles), Figure 4a shows that the contributions to the hazard from the B faults dominate the hazard calculation. Sim-

Table 1

Fault Parameters and Uncertainties from Jackson *et al.* (1995) and Petersen *et al.* (1996) as used in the Monte Carlo Procedure. *L* = Fault Length (km), LSD = Length's SD (km), *W* = Fault width (km), WSD = Width's SD (km), SR = Fault Slip Rate (mm/yr), SRSD = Slip Rate SD (mm/yr), FC = Fault Class (A or B), FT = Faulting Type (SS, Strike Slip; or RS, Reverse Slip), Dip = Fault Dip, Daz = Down Dip Azimuth from North (clockwise), Rtop = Depth to Top of Rupture (km), and Rbot = Depth to Bottom of Rupture (km)

Fault/Segment	L	LSD	W	WSD	SR	SRSD	FC	FT	Dip	Daz	Rtop	Rbot
San Andreas (Cascade Model):												
Carrizo	121	6	11	2	20.12	5.031	A	SS	90.	0.	0.	11.
Mojave	133	6	11	2	17.18	4.295	A	SS	90.	0.	0.	11.
San Bernardino	78	4	11	2	13.59	3.398	A	SS	90.	0.	0.	11.
Coachella	114	6	11	2	17.39	4.347	A	SS	90.	0.	0.	11.
Carrizo-Mojave	254	6	11	2	10.91	2.727	A	SS	90.	0.	0.	11.
SanBern.-Coachella	192	6	11	2	7.67	1.918	A	SS	90.	0.	0.	11.
Carrizo-Coachella	446	6	11	2	3.74	0.936	A	SS	90.	0.	0.	11.
San Jacinto (Cascade Model):												
San Bernardino	35	2	11	2	6.84	1.710	A	SS	90.	0.	0.	11.
San Jacinto	45	2	11	2	7.45	1.862	A	SS	90.	0.	0.	11.
Anza	90	5	11	2	6.87	1.717	A	SS	90.	0.	0.	11.
Coyote Creek	40	2	11	2	2.26	0.565	A	SS	90.	0.	0.	11.
Borego	33	2	11	2	2.01	0.502	A	SS	90.	0.	0.	11.
Superstition Mtn.	25	2	11	2	2.12	0.531	A	SS	90.	0.	0.	11.
Superstition Hills	32	2	11	2	1.66	0.415	A	SS	90.	0.	0.	11.
SanBern.-SanJacinto	80	4	11	2	3.58	0.896	A	SS	90.	0.	0.	11.
CoyoteCk-Sprst.Hlls	105	5	11	2	0.66	0.165	A	SS	90.	0.	0.	11.
SanBern.-Sprst.Mtn	268	6	11	2	1.94	0.484	A	SS	90.	0.	0.	11.
SanBern.-Sprst.Hlls	275	6	11	2	1.76	0.440	A	SS	90.	0.	0.	11.
Elsinore (Cascade Model):												
Whittier	38	2	11	2	1.44	0.361	A	SS	90.	0.	0.	11.
Glen Ivy	35	2	11	2	2.90	0.726	A	SS	90.	0.	0.	11.
Temecula	42	2	11	2	2.82	0.704	A	SS	90.	0.	0.	11.
Julian	75	4	11	2	0.10	0.024	A	SS	90.	0.	0.	11.
Coyote Mtn.	117	6	11	2	0.82	0.205	A	SS	90.	0.	0.	11.
Julian-CoyoteMtn.	113	6	11	2	1.78	0.445	A	SS	90.	0.	0.	11.
GlenIvy-Julian	152	6	11	2	1.45	0.363	A	SS	90.	0.	0.	11.
GlenIvy-CoyoteMtn.	190	6	11	2	0.28	0.070	A	SS	90.	0.	0.	11.
Whittier-CoyoteMtn.	228	6	11	2	1.31	0.327	A	SS	90.	0.	0.	11.
Newport-Inglewood	66	3	11	2	1.0	0.25	B	SS	90.	0.	0.	11.
Offshore Zone of Deformation	50	2	11	2	1.5	0.25	B	SS	90.	0.	0.	11.
Big Pine	45	2	11	2	0.8	0.35	B	SS	90.	0.	0.	11.
Cucamonga	24	2	11	2	5.0	0.5	B	RS	45.	0.	1.	12.
San Antonio Canyon	15	1	11	2	0.5	0.15	B	SS	90.	0.	0.	11.
Sierra Madre	63	7	11	2	3.0	0.5	B	RS	45.	0.	1.	12.
San Gabriel	73	4	11	2	1.0	0.25	B	SS	90.	0.	0.	11.
Holser	16	4	11	2	0.4	0.1	B	RS	45.	0.	1.	12.
Malibu Coast	30	5	11	2	0.5	0.15	B	RS	60.	0.	1.	12.
Santa Monica	39	3	11	2	1.0	0.25	B	RS	55.	0.	1.	12.
Hollywood	18	2	11	2	1.0	0.25	B	RS	60.	0.	1.	12.
Raymond	22	3	11	2	1.0	0.25	B	SS	90.	0.	0.	11.
Palos Verdes	83	7	11	2	3.0	0.5	B	SS	90.	0.	0.	11.
Arroyo Parida–Santa Anna	65	7	11	2	0.4	0.1	B	RS	60.	0.	1.	12.
Santa Ynez	134	8	11	2	1.0	0.25	B	SS	90.	0.	0.	11.
Oak Ridge	97	5	11	2	4.0	0.5	B	RS	65.	180.	1.	12.
Red Mountain	39	2	11	2	2.0	0.5	B	RS	70.	350.	1.	12.
San Cayetano	45	3	11	2	6.0	1.5	B	RS	60.	10.	1.	12.
Santa Susana	32	4	11	2	5.0	1.0	B	RS	55.	0.	1.	12.
Ventura–Pitas Pt.	52	6	11	2	1.0	0.25	B	RS	75.	0.	1.	12.
Simi–Santa Rosa	36	5	11	2	0.7	0.15	B	RS	60.	0.	1.	12.
Elysian Park Thrust	41	4	11	2	1.5	0.5	B*	RS	20.	30.	10.	15.
Compton Thrust	40	4	11	2	1.5	0.5	B*	RS	20.	30.	10.	15.
Northridge Thrust	31	5	11	2	1.5	0.5	B*	RS	42.	180.	5.	20.

*Blind thrust.

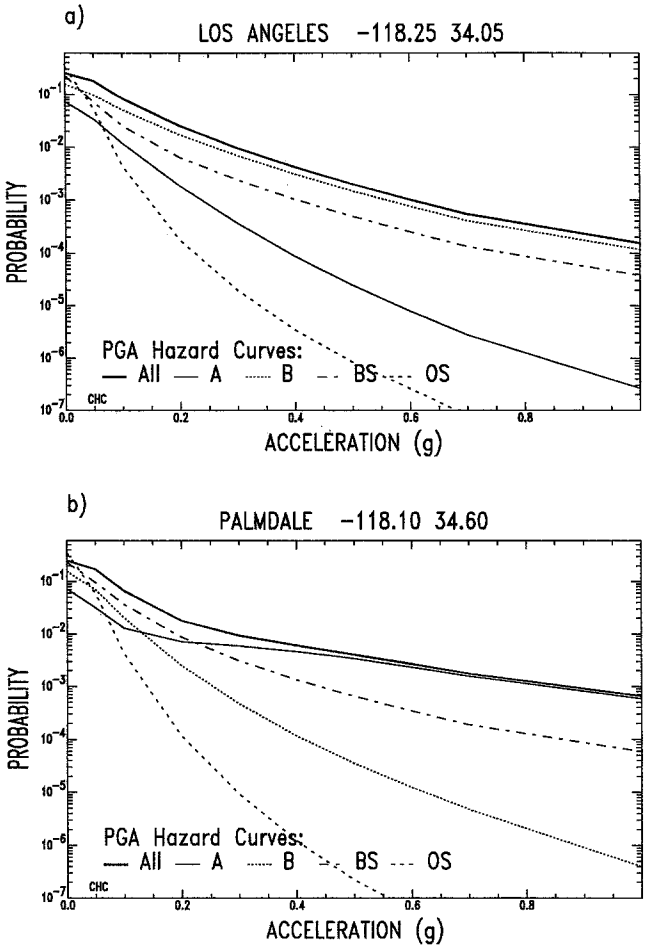

Figure 4. Site-specific PGA hazard curves for (a) Los Angeles and (b) Palmdale (see Fig. 1 for site locations). The thick solid line is the overall hazard curve for the site, the narrow solid line is the A faults only hazard curve, the dotted line is the B faults only hazard curve, the dash-dot line is the hazard curve for the background seismicity within the tri-county area, and the dashed line is the hazard curve for all the seismic sources outside the tri-county area.

ilarly, for sites closer to the A faults (e.g., Palmdale), the contributions to the hazard from the A faults dominate the hazard calculation (Fig. 4b).

The hazard due to the background seismicity within the tri-county area is lower than that due to the dominating faults (either A or B), except for probabilities greater than 0.007 in Figure 4b. Figure 4 suggests that the background seismicity contribution to the uncertainty is relatively small for a probability of 0.0021 (10% in 50 yr). Additionally, Jackson *et al.* (1995) do not provide any estimate of the uncertainty in the calculation of SCEC's background seismicity rates, which where also used in the DMG model. In this article, uncertainty due to background seismicity is not assessed. Cao *et al.* (1996) have assessed the effect of uncertainties in background seismicity on estimates of seismic hazard for southern California. The uncertainty due to seismic sources outside the tri-county area is also ignored because Figure 4 demonstrates their insignificant contribution to the hazard. Thus, the uncertainty assessment in this article is only for the geologic faults in Petersen *et al.*'s PSHA model.

In the Monte Carlo simulations, a series of hazard maps are generated by randomly varying the input parameters to the source model. For each point on the map, the series of hazard values generated by the Monte Carlo runs are sorted into ascending order, and the 2nd, 50th, and 98th percentiles are determined. By definition, 95% of the hazard values in a distribution falls between the 2.5 and 97.5 percentiles, and these percentiles are referred to as the 95% confidence limits for the uncertainty about the median value. The 95% confidence limits represent ± 2 standard deviations for a normal distribution. In this article, the 95% confidence limits are approximated using the 2nd and 98th percentiles.

To generate an uncertainty map, the largest difference between the 50th and 2nd percentiles and the 98th and 50th percentiles is selected to represent two standard deviations (2SD) for the distribution. McGuire and Shedlock (1981) used the coefficient of variation (COV) (SD/mean) to map seismic hazard uncertainty in the San Francisco Bay area. For the tri-county area, other forms of the uncertainty map show similar patterns to the 2SD factor map and present the same information but have smaller amplitudes. The 2SD factor map described above was selected to represent the uncertainty because it provides a better insight into the range in hazard values one can expect than a 1SD map, and it indicates the value to be added or subtracted from the hazard map value to obtain the 95% confidence limits, which is easier for less experienced users to understand than a COV map.

The number of Monte Carlo simulations that make up the series of hazard maps used in generating the percentile statistics is important to the reliability of the uncertainty estimates. This is demonstrated in Figure 5, which shows the 2nd, 16th, 50th, 84th, and 98th percentile values of PGA at one site for two different starting points in the random number table, and for 20, 50, 100, and 500 Monte Carlo simulations. Figure 5 indicates that a minimum of 100 simulations is needed to obtain estimates of ground-motion uncertainty within 5% of each other when different starting points are used in the random number table. Because of the long computer time required to generate the uncertainty map, the minimum of 100 simulations was selected for our Monte Carlo study.

To provide quality control for the results of our study, published computer programs were used for the random number generation, the hazard calculations, and the ranking of hazard values at each site. A modified version of FRISK (McGuire, 1978) was used for the hazard calculations. Routines for sorting (SORT) and random number generation (RAN1 and GASDEV) were taken from Press *et al.* (1992).

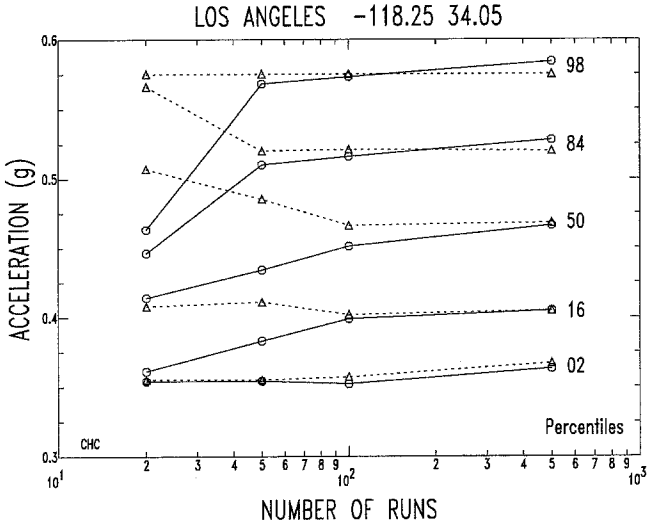

Figure 5. The 98th, 84th, 50th, 16th, and 2nd percentile values from PGA uncertainty distributions for 20, 50, 100, and 500 Monte Carlo simulations. Hexagons are for one entry point to the random number table, and triangles are for a different entry point to the random number table. Lines connect common percentile values among the different number of simulations (solid lines for the hexagons and dashed lines for the triangles).

Results and Discussion

Intramodel Uncertainty

Figure 6a presents a map of the overall uncertainty from the nine parameters listed in Figure 3. The mapped value is the 95% confidence factor (2SD) in units of acceleration (i.e., g) about the expected value of PGA (10% exceedence in 50 yr) shown in Figure 2. The contour interval for Figure 6a is 0.1 g. The estimated uncertainty can be as large as $\pm 50\%$ of the expected value of Figure 2. Comparing Figures 2 and 6a indicates that the overall uncertainty is about the same percentage near the A faults (San Andreas, San Jacinto, and Elsinore) as the B faults (other faults shown in Fig. 1).

For comparison with other published uncertainty analyses, an alternate presentation of the overall uncertainty is presented in Figure 6b, using coefficient of variation (COV). The maximum COV is 0.28 with high values (>0.2) predominately over the San Andreas Fault and the Transverse Ranges. Values of COV decrease with increasing distance from the faults as previously demonstrated for the San Francisco Bay area by McGuire and Shedlock (1981). Because background seismicity is not included in this article, the decrease in COV with distance does not level off in Figure 6b. Cao *et al.* (1996) determined a general COV value of 0.24 for the seismic hazard uncertainty due to background seismicity in southern California. This suggests that at distances far enough from faults for background seismicity to dominate the hazard, values of COV should return to 0.24.

McGuire and Shedlock (1981) show COV values ranging from about 0.4 near faults to about 0.2 away from faults for the San Francisco Bay area. Clearly, their values of COV are higher than those we obtain for southern California. This difference is explained by McGuire and Shedlock's use of discrete distributions with larger variances. For example, the three attenuation relations used by McGuire and Shedlock are based on less data and have more intrarelation (aleatory) and interrelation (epistemic) variance than the attenuation relations used in this article and accounts for much of the difference in COV. (McGuire and Shedlock used a natural logarithmic aleatory uncertainty of 0.62 for all three of their relations, while for large events, the aleatory uncertainty for our three relations is 0.52, 0.40, and 0.39. For a rock site 10 km from a $M7.0$ strike-slip event, McGuire and Shedlock's epistemic uncertainty is 0.53 ± 0.20 g, and ours is 0.35 ± 0.06 g.) Also, McGuire and Shedlock used three discrete branches for each parameter that can emphasize more extreme values than the continuous distributions used in this article. An example of a discrete distribution that emphasizes extreme values from this article is the discrete choice of either characteristic or Gutenberg–Richter magnitude distribution for B faults. Future modeling of earthquake magnitude distributions as $X\% \pm Y\%$ characteristic instead of one extreme or the other should further reduce COV's just as the use of continuous parameter distributions and the reduction of variance in attenuation relations reduced COV's in this article from those of McGuire and Shedlock.

Figures 7a through 7i present the contribution of each of the nine parameters alone to the overall uncertainty of Figure 6, in descending order of significance. As in Figure 6a, the uncertainty is presented in Figures 7a through 7i as the 95% confidence factor. The contour interval for Figures 7a through 7f is 0.05 g and for Figures 7g through 7i is 0.025 g. While one of the nine parameters is being varied, the other eight parameters were held fixed. For the continuous distribution parameters, the value held fixed is the mean value of the distribution. For the discrete distribution, the fixed values are Boore *et al.* for the attenuation relation, Gutenberg–Richter for the magnitude-frequency distribution, and blind thrusts included for the Los Angeles area.

Generally, uncertainties in the rupture length versus magnitude relation, the choice of attenuation relation, the magnitude distribution for B faults, and the slip rates have a large contribution to the overall uncertainty. Uncertainties in the fault width and b-value have a moderate but significant contribution. And uncertainties in the fault length and shear modulus have a very small contribution.

In detail, the maps of Figure 7 show some variation in the results depending on whether a site is near an A or B fault. Sites near A faults and blind thrusts are more affected by the uncertainty in the rupture length versus magnitude relation of Wells and Coppersmith (1994) than sites near B faults (Fig. 7a), because characteristic faults are more sensitive to the maximum magnitude earthquake determined from that relationship. Also, sites near A faults are more affected by the uncertainty in the choice of attenuation re-

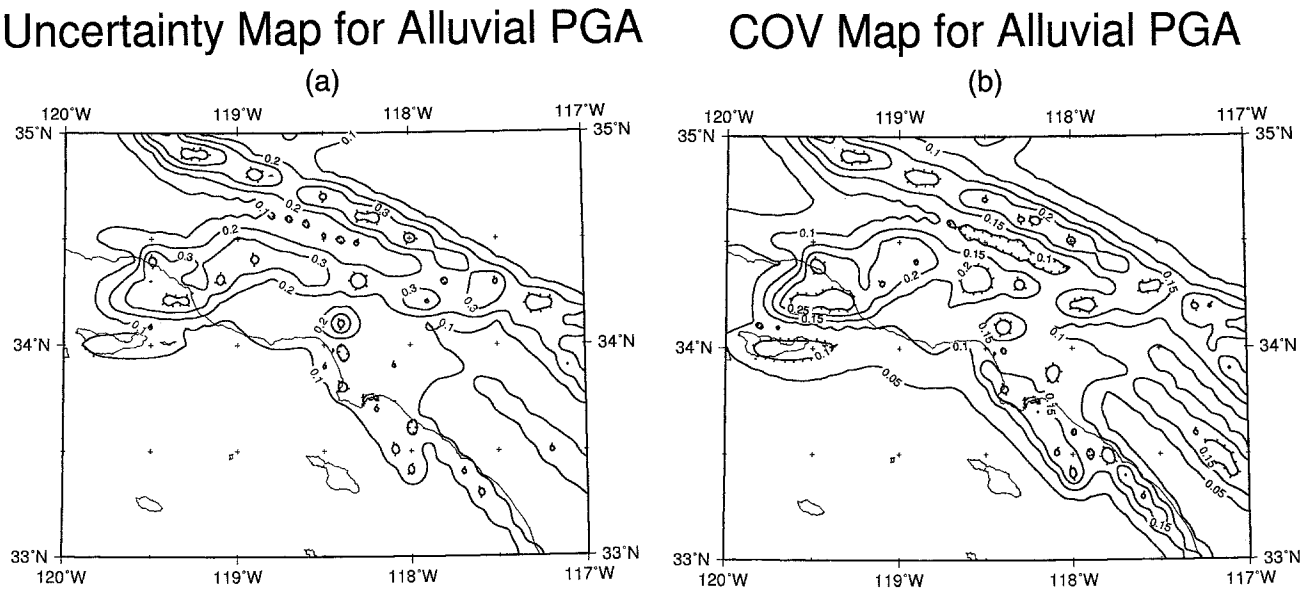

Figure 6. (a) The overall PGA uncertainty factor map (±95% confidence level value) for the hazard map shown in Figure 2. The contour interval is 0.1 *g*. (b) The corresponding coefficient of variation map with a contour interval of 0.05.

lationship and in the shear modulus than sites near B faults (Fig. 7b and 7i). Uncertainty in the magnitude distribution (characteristic versus Gutenberg-Richter) and in the *b*-value only affects sites near B faults (Figs. 7c and 7f) because A faults always have a characteristic magnitude distribution that by definition is insensitive to *b*-value. In Figure 7d, the effect of uncertainty in slip rate is dependent only on the amplitude of the slip-rate uncertainty.

From Figures 7a through 7i, the major contributors to the overall uncertainty vary depending on whether a site is near an A fault or a B fault. But, from Figures 2 and 6a, the overall uncertainty is about the same for A and B faults, percentage wise (up to ±50%). For sites near A faults (characteristic magnitude distribution only), the major contributors are the uncertainty in maximum magnitude for the characteristic event (Wells and Coppersmith relations), the uncertainty in the choice of attenuation relation, and the uncertainty in the slip rates. For sites near B faults, the major contributor is the uncertainty in the choice of magnitude-frequency distribution, followed closely (for the Gutenberg–Richter distribution) by the uncertainty in the Wells and Coppersmith relations, the uncertainty in the choice of attenuation relation, and in the uncertainty in slip rates. Also, some contribution is made by the uncertainty in *b*-value and the uncertainty in fault width.

How Uncertainty Depends on Hazard Value

The overall uncertainty depends on the amplitude of the ground-motion hazard. This dependence results from the four major contributors to the overall uncertainty: maximum magnitudes, attenuation relations, type of magnitude distribution, and slip rates. The reason for each of the four parameter's dependence on the value of the hazard is explained below.

The formulas for determining the rate of earthquakes on a fault from geologic information are needed to explain a portion of the observed dependence on hazard value. From Anderson and Luco (1983) (type 2 equation) and Youngs and Coppersmith (1985), the formulas for annual rates of earthquakes, based on geologic information, are

$$\text{rate}_{\text{char}} = u \cdot L \cdot W \cdot \text{SR}/10^{c*mu+d}, \quad (1)$$

and

$$\text{rate}_{g-r}(mo) = \text{rate}_{\text{char}} \cdot (10^{b*(mu-mo)} - 1) \cdot (c - b)/b. \quad (2)$$

$\text{Rate}_{\text{char}}$ and rate_{g-r} are the annual rates of earthquakes for characteristic and Gutenberg–Richter fault behavior, respectively; u is shear modulus; L is fault length; W is fault width; SR is slip rate; c and d are from the moment-magnitude relation ($\log M_o = c*M_w + d$); b is *b*-value; *mu* is the characteristic or maximum magnitude from Wells and Coppersmith relations; and *mo* is the minimum magnitude of the Gutenberg–Richter distribution.

How maximum magnitude causes a hazard dependent uncertainty is apparent from the exponential dependence on *mu* in equations (1) and (2). The exponential dependence of rates of earthquakes on *mu* makes the overall hazard uncertainty proportional to the value of *mu*. From Table 1 and Figures 1 and 2, for each type of magnitude-frequency distribution (characteristic or Gutenberg–Richter), the faults

Rupture Length vs Magnitude Only

(a)

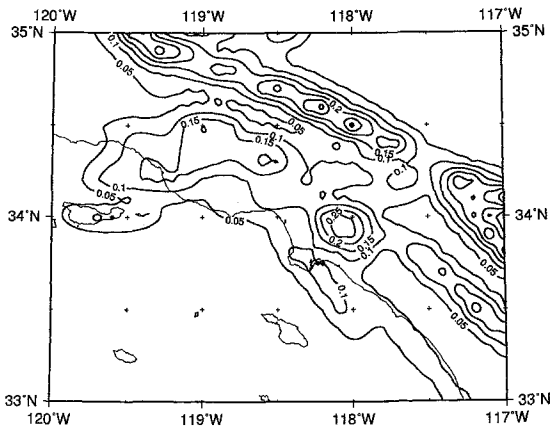

Attenuation Relation Uncertainty Only

(b)

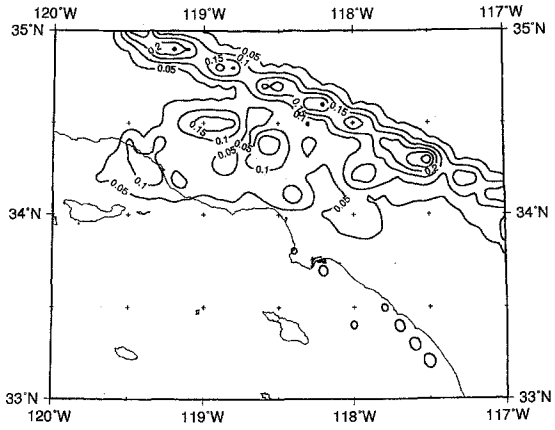

B Fault's Magnitute Distribution Only

(c)

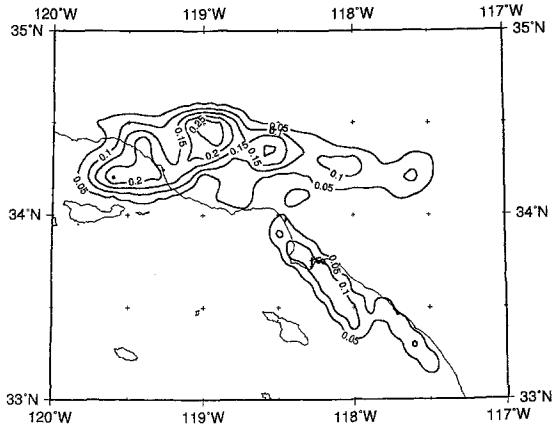

Slip Rate Uncertainty Only

(d)

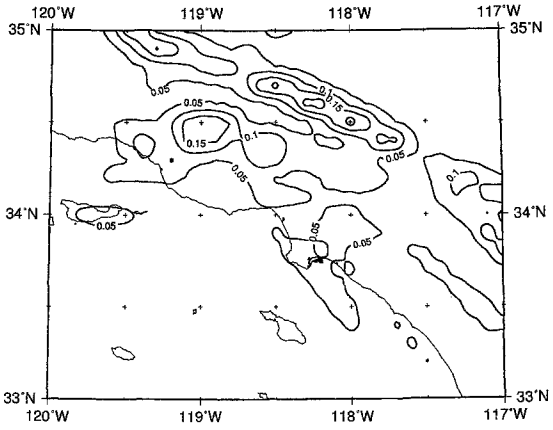

Width Uncertainty Only

(e)

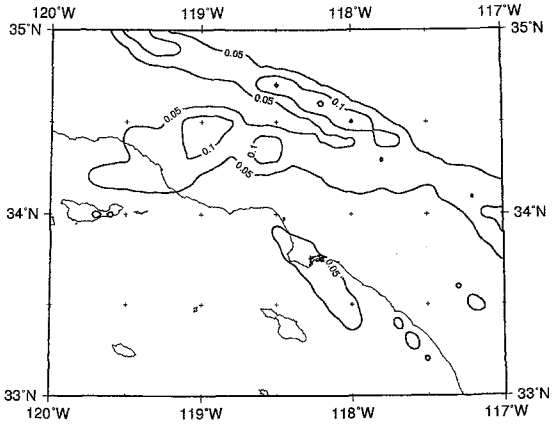

B-value Uncertainty Only

(f)

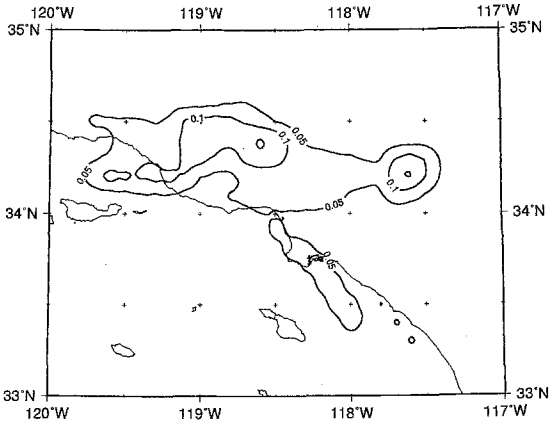

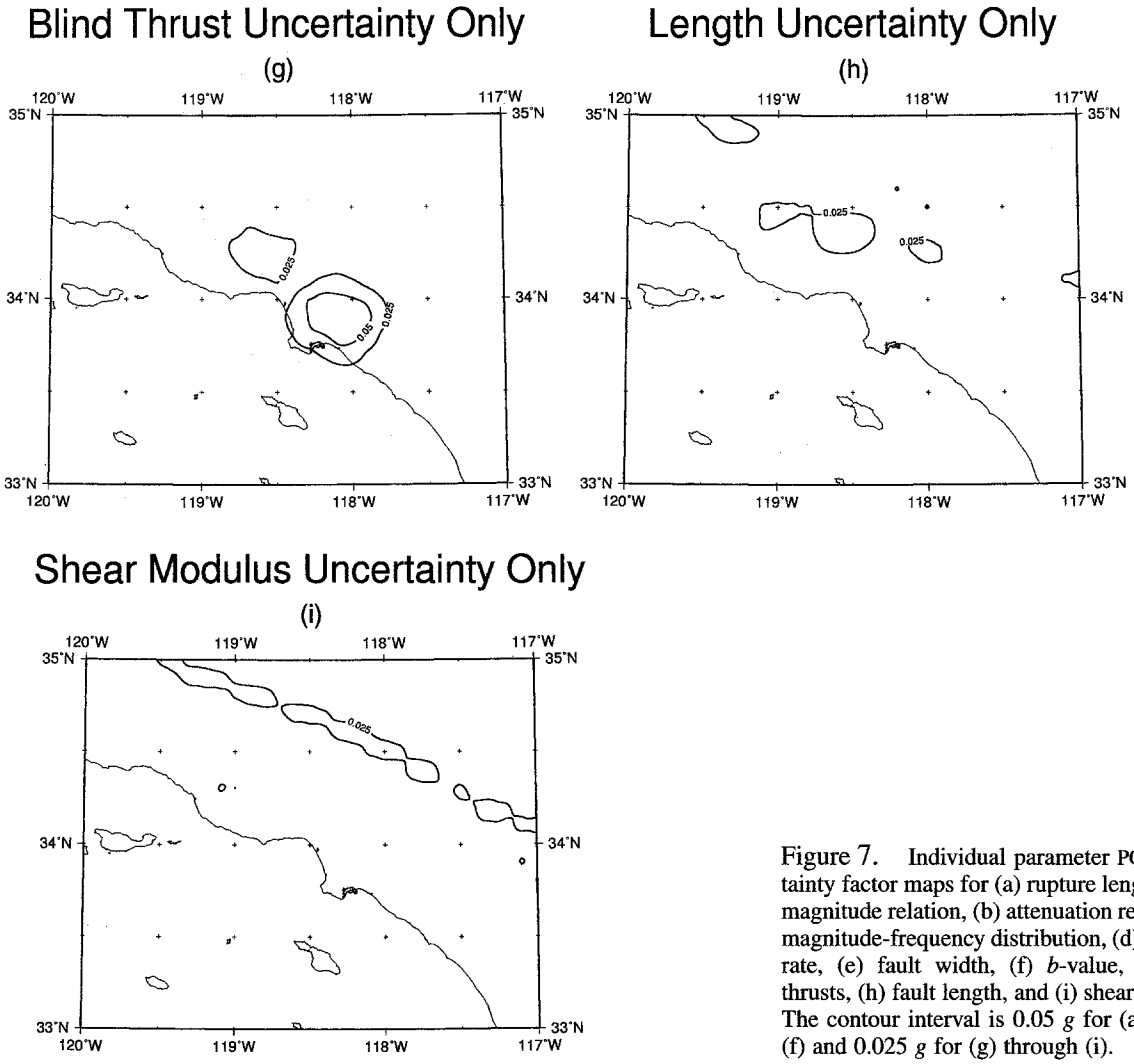

Figure 7. Individual parameter PGA uncertainty factor maps for (a) rupture length versus magnitude relation, (b) attenuation relation, (c) magnitude-frequency distribution, (d) fault slip rate, (e) fault width, (f) *b*-value, (g) blind thrusts, (h) fault length, and (i) shear modulus. The contour interval is 0.05 *g* for (a) through (f) and 0.025 *g* for (g) through (i).

with the largest lengths have the largest *mu* and hazard, hence larger uncertainties in Figure 7a.

How differing attenuation relations cause a hazard-dependent uncertainty is evident from the epistemic uncertainty among attenuation relations. Close in to a fault, the difference in hazard values computed using various attenuation relations increases with magnitude. This is due to the different form, input ground-motion data, and distance measure used by each attenuation relation (epistemic uncertainty). In general, the longer faults generate larger-magnitude earthquakes and have a larger moment release. Thus, for a given type of magnitude-frequency distribution, longer faults tend to have a larger hazard and a larger variance in hazard among attenuation relations. This is illustrated in Figure 7b.

Equations (1) and (2) again explain how a B fault's uncertainty in magnitude distribution causes a hazard-dependent uncertainty. The Gutenberg–Richter distribution produces a higher hazard close to a given fault than a characteristic distribution. From equation (2), the ratio $\text{rate}_{g-r}/\text{rate}_{\text{char}}$ increases exponentially as *mu* increases (fault length increases). Thus, as fault length increases, both the hazard and the ratio $\text{rate}_{g-r}/\text{rate}_{\text{char}}$ increase, which implies a proportional increase in the difference in hazard between Gutenberg–Richter and characteristic magnitude distributions. Hence there is a larger uncertainty with increasing hazard, as shown in Figure 7c.

How slip rates cause a hazard-dependent uncertainty is apparent from the slip-rate uncertainty values in Table 1. In equations (1) and (2), rates of earthquakes are directly proportional to slip rates. This means that the uncertainty in rates of earthquakes are dependent on the size of the uncertainty in slip rates but not on the value of slip rate ($\Delta\text{rate} = \text{const}*\Delta\text{SR}$). Unfortunately, in Table 1, the faults with the largest slip rates also tend to have larger absolute uncertainties in their slip rates and hence a larger uncertainty contribution in Figure 7d. If the faults in Table 1 had the same value of slip-rate uncertainty, the dependence on slip-rate values would disappear from Figure 7d.

Therefore, the four major contributors to overall uncertainty exhibit an uncertainty that is dependent on the value

of the hazard. This explains the overall uncertainty's dependence on hazard value.

Intermodel Uncertainty

Shifting to intermodel geologic uncertainties, Figure 7g shows the effect of including or excluding blind thrusts in the Los Angeles area. Petersen *et al.* (1996) weighed blind thrusts by 50% because of their uncertainty in geometry and activity rates compared to those faults that are observed at the surface. The uncertainty of including blind thrusts in the model or not is expressed in Figure 3 by a choice to include or exclude them. From Figure 7g, the uncertainty due to the presence or absence of blind thrusts is very small, mainly because the slip rates for the blind thrusts are relatively low (1.5 mm/yr) compared with other adjoining faults.

Jackson *et al.* (1995) report both a cascade (multi-segment and single-segment ruptures) and a noncascade (single-segment ruptures only) model for the A faults in southern California. Figure 8 presents just the uncertainty between the cascades and noncascades models. From Figure 8, it is clear that there is very little uncertainty contribution (<0.1 *g* at the 95% confidence level) to the overall uncertainty if a cascades/noncascades branch were to be added to the logic tree of Figure 3. In terms of hazard, there is little difference between these two models.

However, if a segmented fault is replaced by a single fault in the model, there is a significant difference in the resulting hazard. For example, consider a model where the fault segmentation of Figure 1 and Table 1 is replaced with unsegmented San Andreas, San Jacinto, and Elsinore faults, a combined Santa Susana–Sierra Madre–Cucamonga fault, a combined Arroyo Parida–Santa Anna–San Cayetano–Holser fault, one long Garlock fault (instead of two segments), a combined Newport–Inglewood–Offshore–Rose Canyon fault, and a Santa Cruz Island extended eastward to just south of Point Dume. Figure 9 shows the intermodel uncertainty between the segmented and unsegmented models, assuming characteristic fault behavior in both models. While the eastward extension of the Santa Cruz Island fault has a small effect (0.05 *g* at the 95% confidence level), combining segments for the other faults has a large effect on the calculated hazard, especially for the A faults in Table 1. The exception is the Newport–Inglewood–Offshore–Rose Canyon combined fault because of their lower slip rates (~1.0 mm/yr). Large changes in segmentation length in a model have an important affect on the uncertainty in the hazard calculation.

The uncertainty in the placement of segments along a given fault is not explicitly addressed in this article. But because the uncertainty in the placing of segments along a fault only produces relatively small changes in segment length (~10 km), the above sensitivity results suggest the affect is small.

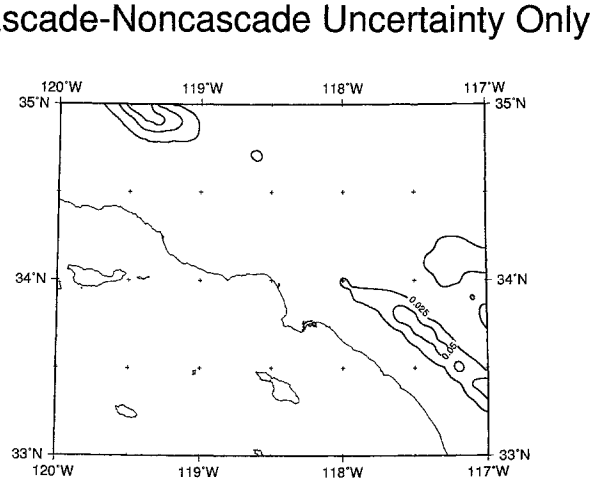

Figure 8. Intermodel PGA uncertainty factor map for cascades versus noncascades models. The contour interval is 0.025 *g*.

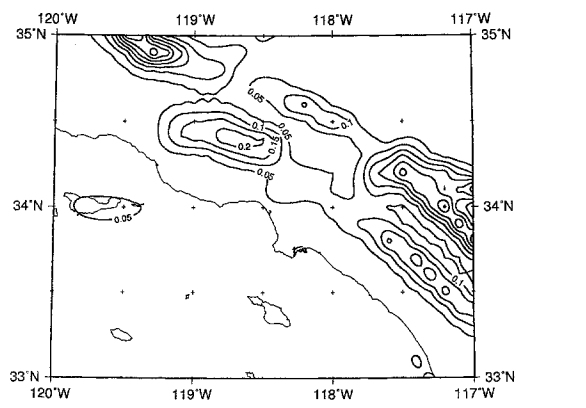

Figure 9. Intermodel PGA uncertainty factor map for segmented versus single large-fault models. The contour interval is 0.05 *g*.

Summary

A Monte Carlo logic tree approach has been successfully applied to the uncertainty analysis of a PSHA model for a tri-county area of southern California (Los Angeles, Orange, and Ventura counties). The intramodel uncertainty in PGA hazard estimates near faults with characteristic behavior or with Gutenberg–Richter behavior is dominated by the uncertainty in (1) the Wells and Coppersmith (1994) relations (uncertainty in the magnitude of the characteristic events), (2) the choice of attenuation relation, and (3) the slip rate. Additionally, a major contributor to the intramodel uncertainty in PGA hazard estimates near faults where the magnitude-frequency relation could be either the Gutenberg–Richter or the characteristic model is the uncertainty in the magnitude-frequency relation. Intermodel uncertainty

is very small for the modeling options of including blind thrusts in the Los Angeles area or of cascading segments along the San Andreas, San Jacinto, and Elsinore faults. Despite variations in the contributors to the overall uncertainty estimates, overall uncertainty is up to $\pm 50\%$ for the DMG hazard model for the tri-county area of southern California.

Acknowledgments

The authors thank Norm Abrahamson, David Boore, and Tianqing Cao for important discussions and Dave Jackson, Robin McGuire, David Perkins, and Tousson Toppozada for critical reviews of the manuscript. These led to significant improvements in the article. We also acknowledge the use of the Generic Mapping Tools software package by Wessel and Smith (1991) to generate Figures 2 and 6 through 9.

References

Anderson, J. G. and J. E. Luco (1983). Consequences of slip rate constraints on earthquake occurrence relations, *Bull. Seism. Soc. Am.* **73,** 471–496.

Boore, D. M., W. B. Joyner, and T. E. Fumal (1993). Estimation of response spectra and peak accelerations from western North American earthquakes: an interim report, *U.S. Geol. Surv. Open-File Rept. 93-509,* 72 pp.

Boore, D. M., W. B. Joyner, and T. E. Fumal (1994). Estimation of response spectra and peak accelerations from western North American earthquakes: an interim report, Part 2, *U.S. Geol. Survey Open-File Rept. 94-127,* 40 pp.

Campbell, K. W. and Y. Bozorngia (1994). Near-source attenuation of peak horizontal acceleration from worldwide accelerograms recorded from 1957 to 1993, in *Proc. of the Fifth U.S. National Conference on Earthquake Engineering,* July 10–14, 1994, Vol. 3, Chicago, Illinois, Earthquake Engineering Research Institute, Oakland, California, 283–292.

Cao, T., M. Petersen, and M. Reichle (1996). Seismic hazard assessment from background seismicity in southern California, *Bull. Seism. Soc. Am.* **86,** 000–000.

Coppersmith, K. J. and R. R. Youngs (1986). Capturing uncertainty in probabilistic seismic hazard assessments within interplate tectonic environments, in *Proc. of the Third U.S. National Conference on Earthquake Engineering,* August 24–28, 1986, Charleston, South Carolina, Vol. 1, Earthquake Engineering Research Institute, Oakland, California, 301–312.

Hanks, T. C. and H. Kanamori (1979). A moment magnitude scale, *J. Geophys. Res.* **84,** 2348–2350.

Jackson, D. D. *et al.* (1995). Seismic hazards in southern California: probable earthquakes, 1994–2024, *Bull. Seism. Soc. Am.* **85,** 378–439.

McGuire, R. K. (1978). FRISK: computer program for seismic risk analysis using faults as earthquake sources, *U.S. Geol. Surv. Open-File Rept. 78-1007,* 71 pp.

McGuire, R. K. and K. M. Shedlock (1981). Statistical uncertainties in seismic hazard evaluations in the United States, *Bull. Seism. Soc. Am.* **71,** 1287–1308.

NRC (1988). *Probabilistic Seismic Hazard Analysis,* National Academy Press, Washington, D.C., 97 pp.

Petersen, M. D., C. H. Cramer, W. A. Bryant, M. S. Reichle, and T. R. Toppozada (1996). Preliminary seismic hazard assessment for Los Angeles, Ventura, and Orange counties, California, effected by the January 17, 1994 Northridge earthquake, *Bull. Seism. Soc. Am.,* S247–S261.

Press, W. H., S. A. Teukolsky, W. T. Vetterling, and B. P. Flannery (1992). *Numerical Recipes in FORTRAN, the Art of Scientific Computing,* 2nd ed., Cambridge University Press, New York, 963 pp.

Reasenberg, P. A. and L. M. Jones (1989). Earthquake hazard after a mainshock in California, *Science* **243,** 1173–1176.

Ward, S. N. (1994). A multidisciplinary approach to seismic hazard in southern California, *Bull. Seism. Soc. Am.* **84,** 1293–1309.

Wells, D. L. and K. J. Coppersmith (1994). New empirical relationships among magnitude, rupture length, rupture width, rupture area, and surface displacement, *Bull. Seism. Soc. Am.* **84,** 974–1002.

Wessel, P. and W. H. F. Smith (1991). Free software helps map and display data, *EOS* **72,** 441, 445–446.

Youngs, R. R. and K. J. Coppersmith (1985). Implications of fault slip rates and earthquake recurrence models to probabilistic seismic hazard estimates, *Bull. Seism. Soc. Am.* **75,** 939–964.

Department of Conservation
Division of Mines and Geology
801 K Street, MS 12-31
Sacramento, California 95814-3531

Manuscript received 7 November 1995.